AIRS Near-Real-Time Products and Algorithms in Support of Operational Numerical Weather Prediction

Mitchell D. Goldberg, Yanni Qu, Larry M. McMillin, Walter Wolf, Lihang Zhou, and Murty Divakarla

***Abstract*—The assimilation of Atmospheric InfraRed Sounder, Advanced Microwave Sounding Unit-A, and Humidity Sounder for Brazil (AIRS/AMSU/HSB) data by Numerical Weather Prediction (NWP) centers is expected to result in improved forecasts. Specially tailored radiance and retrieval products derived from AIRS/AMSU/HSB data are being prepared for NWP centers. There are two types of products—thinned radiance data and full-resolution retrieval products of atmospheric and surface parameters. The radiances are thinned because of limitations in communication bandwidth and computational resources at NWP centers. There are two types of thinning: 1) spatial and spectral thinning and 2) data compression using principal component analysis (PCA). PCA is also used for quality control and for deriving the retrieval first guess used in the AIRS processing software. Results show that PCA is effective in estimating and filtering instrument noise. The PCA regression retrievals show layer mean temperature (1 km in troposphere, 3 km in stratosphere) accuracies of better than 1 K in most atmospheric regions from simulated AIRS data. Moisture errors are generally less than 15% in 2-km layers, and ozone errors are near 10% over approximately 5-km layers from simulation. The PCA and regression methodologies are described. The radiance products also include clear field-of-view (FOV) indicators. The residual cloud amount, based on simulated data, for FOVs estimated to be clear (free of clouds) is about 0.5% over ocean and 2.5% over land.**

***Index Terms*—Atmospheric retrieval, atmospheric soundings, eigenvectors, hyperspectral, infrared, microwave, principal components, satellite remote sensing.**

I. Introduction

THE Atmospheric InfraRed Sounder (AIRS) is the first of a new generation of high spectral resolution infrared sounder with 2378 channels measuring outgoing radiance between 650 and 2675 cm^{-1}. The improved vertical resolving power of the AIRS is expected to greatly improve the accuracy of temperature and moisture soundings. Details on the AIRS instrument and performance are given in [1], [2]. The AIRS is accompanied by two microwave sounders, the Advanced Microwave Sounding Unit-A (AMSU-A) and Humidity Sounder for Brazil (HSB) [2]. AIRS temperature and moisture soundings (retrievals) will have vertical resolutions of 1–2 km, instead of 3–5 km from current National Oceanic and Atmospheric Administation (NOAA) operational sounders—such as the High Resolution Infrared Sounder (HIRS) [3], AMSU-A and AMSU-B. The three NOAA instruments are often referred to as the Advanced TIROS Operational Vertical Sounder (ATOVS). The HSB is essentially the same as the NOAA AMSU-B instrument without the 89-GHz channel. Details of the NOAA ATOVS instruments can be found in [4]. Because forecast skill is dependent on the quality of the information that is assimilated into the forecast model, AIRS/AMSU/HSB products are expected to improve weather forecasts [5]. Over the past decade there have been many improvements in the assimilation of satellite data into forecast models. Major NWP centers have replaced atmospheric temperature and moisture soundings (i.e., retrievals) in forecast models with directly assimilated calibrated clear radiances [6]–[9]. For current operational sounders, assimilating radiances from 20 or so channels and not having to account for a retrieval's vertically and horizontally correlated errors is very attractive. However, it becomes less attractive with 2000+ AIRS channels. Even though major NWP centers will assimilate radiances, the retrieval products are needed by forecast centers assimilating retrievals and by those studying differences between radiance and retrieval assimilation (e.g., Goddard's Data Assimilation Office). Retrievals can be an important source of information for nowcasting applications and for validation of model analyses and forecasts. For severe weather forecasting applications, three-dimensional thermal and moisture fields at the sounder resolution and in near-real-time can provide important diagnostic information.

In 1999, there was a significant improvement in forecast skill due to the assimilation of radiances from the AMSU-A onboard NOAA-15 and NOAA-16 satellites [9]–[11]. The first AMSU-A on NOAA-15 was launched in 1998. The improvement can be traced to two main reasons. First, the AMSU-A has very good vertical coverage, although not vertical resolution, from the surface to the upper stratosphere. Second, a large percentage ($>90\%$) of the data can be assimilated, since most of the microwave atmospheric sounding channels are not sensitive to nonprecipitating clouds. Prior to AMSU-A, the primary observations for sounding the atmosphere were from the HIRS. Only 10% of HIRS data are assimilated due to cloud contamination. The improvement in 1999 was mostly due to the use of AMSU-A in cloudy regions. AIRS observations will provide much better vertical resolution than AMSU-A and HIRS combined, but are still affected by clouds. It is important how AIRS data are assimilated in NWP models. If only clear fields of view (FOVs) are used, then only about 5% of the

Manuscript received April 29, 2002; revised November 8, 2002. This work was carried out at NESDIS and supported by the National Aeronautics and Space Administration, the NOAA Integrated Program Office, and the NOAA/NASA Joint Center for Satellite Data Assimilation.

M. D. Goldberg and L. M. McMillin are with the National Oceanic and Atmospheric Administration, National Environmental Satellite, Data, and Information Service, Office of Research and Applications, Camp Springs, MD 20746 USA.

W. Wolf and L. Zhou are with the QSS Group Inc., Lanham, MD 20706 USA.

Y. Qu and M. Divakarla are with the Decision System Technology Incorporation, Rockville, MD 20850 USA.

Digital Object Identifier 10.1109/TGRS.2002.808307

0196-2892/03$17.00 © 2003 IEEE

data will be assimilated and the forecast impact will likely be limited.

AIRS radiances can be assimilated in the following three forms:

1) radiances that are not affected by clouds;
2) cloud-corrected (cloud-cleared) radiances [12]–[16];
3) cloud-contaminated radiances [17].

As discussed in [16], the coverage expected from AIRS cloud-cleared radiances is at least 50%. The use of cloud-contaminated radiances is strongly dependent on the ability of the NWP model to predict cloud optical properties, so cloud-contaminated radiances are not widely used. While most centers will use clear radiances, consideration should be given to assimilate cloud-cleared radiances because of the much higher yield. With respect to retrievals, the AIRS product generation system will produce retrievals from cloud-cleared radiances. For overcast cases, the retrievals are derived from the AMSU-A and the HSB microwave observations and AIRS observations that are not affected by clouds. A complete description of the retrieval process is described in [1] and [16].

The purpose of this paper is to describe the data that will be provided to NWP centers in near-real-time, generally within three hours from the satellite observation time, and to provide details of algorithms we have developed for the AIRS processing system. Primarily these include tests to determine if an AIRS field of view (FOV) is clear, i.e., free of clouds, and the use of principal components for data compression, quality control, noise filtering and estimation, and regression retrievals. The regression retrieval is used for the first guess in the AIRS final retrieval. The regression retrieval is computationally very fast and can be generated directly from the principal component score dataset, which is available to NWP centers in near-real-time. A fast retrieval may possibly provide NWP centers the capability to find regions over the globe where assimilating AIRS products would be important (i.e., places where the regression retrieval differs greatly from the forecasts). The use of a regression "filter" may be important for those centers where the assimilation of AIRS from all global regions is a computational burden.

II. AIRS Near Real-Time Products

The initial constraint in providing AIRS NWP products in near-real-time is data volume size. AIRS/AMSU/HSB level 1b data are about 2.5 GB for a 100-min orbit in comparison to the approximately 14 MB per orbit from ATOVS (HIRS ~4.5 MB, AMSU-A ~2 MB, AMSU-B ~7.5 MB). Each 6-min granule consists of 90 AIRS and HSB FOVs per scanline and 30 AMSU-A FOVs per scanline. There are 135 AIRS and HSB scanlines per granule, 45 AMSU-A scanlines per granule, and 240 granules per day [1]. A simple solution to the relatively high volume of AIRS/AMSU/HSB is to increase available communication bandwidth. But that option is costly, and presently NWP centers cannot assimilate all the data due to computational costs and limitations in storing the data. So one solution is to thin the radiance data. The level 2 product files will not have to be thinned. The level 2 product includes atmospheric temperature, moisture, and ozone profiles, surface temperature, surface emissivity/reflectivity, and cloud height and amount [1], [16]. The AIRS/AMSU/HSB data will be thinned into several datasets described in Section II-A–D. Each file contains the results of the cloud detection tests discussed in Section III-E. Also each file has ancillary information such as quality indicators, time, latitude, longitude, and satellite and solar viewing geometry.

A. Thinned Radiance Data—Single FOV

A diagram of the FOVs for AIRS, AMSU-A, and HSB and the cross-track scan pattern of the three instruments can be found in [1]. Visually, each AMSU-A FOV, which has a spatial resolution of approximately 42 km on earth near the nadir view position, contains a 3×3 array of AIRS and HSB FOVs, each with a spatial resolution of approximately 14 km. The AIRS and HSB FOVs are spatially coincident. The data are thinned by subsampling FOVs and channels. A subset of about 300 channels (the set has not been finalized) is extracted from the center AIRS FOV of the 3×3 array, as well as all 15 AMSU-A channels and the four HSB channels from the center HSB FOV. Each granule has two files, each containing data from alternate center FOVs. The size of each file is about 0.5 MB. An orbit's worth of data is about 16 MB, which is only about 15% greater than the full ATOVS data. The method of channel selection is described in [16] and retrievals derived from the subset have been shown, in simulation, to satisfy all 2000+ AIRS channels to within the estimated instrument noise.

The single FOV thinned radiance dataset is the core data that will be used by most centers assimilating AIRS radiances. The files are available in BUFR and HDF formats.

B. Thinned Radiance Data—9 FOVs

The number of channels in this dataset is the same as the single FOV radiance dataset. The main difference is that instead of the center FOV, all nine AIRS and HSB FOVs from every other AMSU-A FOV are included. The file size for a 6-min granule is about 4.5 MB, and one orbit's worth of data is about 70 MB. Having all nine FOVs will allow users to generate their own cloud-cleared AIRS radiances. This dataset was specifically requested by the Goddard Data Assimilation Office (DAO).

C. Principal Component Data—Single FOV

The principal component score file is thinned spatially in the same manner as the single FOV radiance file. However, instead of the subset of AIRS channels, there are 200 principal scores. All AIRS channel radiances can be reconstructed to the noise level of AIRS from the principal component scores. Details are provided in Section III-A. A measure of how well the channels can be reconstructed is also provided. This measure, referred to as the reconstruction score, is a single value that gives an overall indication of how well the reconstructed radiances agree with the actual radiances. A reconstruction of less than unity indicates that overall the radiances are reconstructed within the instrument noise level of the observed radiances.

D. Cloud-Cleared Data

The level 2 processing system also generates cloud-cleared radiances and cloud-cleared principal component scores. These data will be available in both HDF and BUFR format and will be very similar in format to those described in Sections II-A and C.

III. Algorithms and Results

This section describes the algorithms that we developed in support of the AIRS radiance and level 2 products. As mentioned earlier the algorithms include 1) principal component analysis for data compression, quality control, noise filtering and noise estimation, and regression level 2 products and 2) AIRS FOV clear detection. The AIRS Science Team developed a simulation package to aid in the development and improvement of algorithms [18]. The simulations include variable surface emissivity and clouds. We have used this simulation package to generate AIRS/AMSU/HSB data in near-real-time since April 2000. The simulated data have been invaluable for developing and testing the processing and distribution systems. The NWP centers benefitted from the real-time simulated data by being able to develop the necessary software needed to assimilate AIRS/AMSU/HSB in advance of the real data.

A. Principal Component Analysis

Principal component analysis (PCA), also called eigenvector decomposition, is often used to approximate data vectors having many elements (e.g., AIRS observations of 2000+ channels) with a new set of data vectors having fewer elements, while retaining most of the variability and information of the original data. The new data vectors are called principal component score vectors, and because they consist of the components of the original data vector in an orthogonal coordinate system, the elements of a given principal component score vector are independent of each other (unlike the original spectrum). Principal component analysis has been used in sounding applications as described in [19] and [20], and recently it has been described in [21] for high spectral resolution infrared sounders. Elements of a principal component score vector are projections of the spectrum onto each of the orthogonal basis vectors, which are the eigenvectors (principal components) of the radiance covariance matrix. The total number n of eigenvectors is equal to the total number of channels. However, it will be shown that a much smaller set of k eigenvectors (<100), ordered from largest to smallest eigenvalues, is sufficient to explain most of the variance in the original spectra. The covariance matrix is derived from an ensemble of AIRS normalized spectra, i.e., radiance divided by the instrument noise. The matrix of eigenvectors $\mathbf{E}$ is related to the covariance matrix $\mathbf{S}$ by

$$\mathbf{S} = \mathbf{E}\mathbf{\Lambda}\mathbf{E}^T \tag{1}$$

where $\mathbf{S}$, $\mathbf{E}$, and $\mathbf{\Lambda}$ are all dimensioned $n \times n$, and $\mathbf{\Lambda}$ is a diagonal matrix of eigenvalues. The principal component scores vector $\mathbf{p}$ is computed from

$$\mathbf{p} = \mathbf{E}^T\mathbf{r} \tag{2}$$

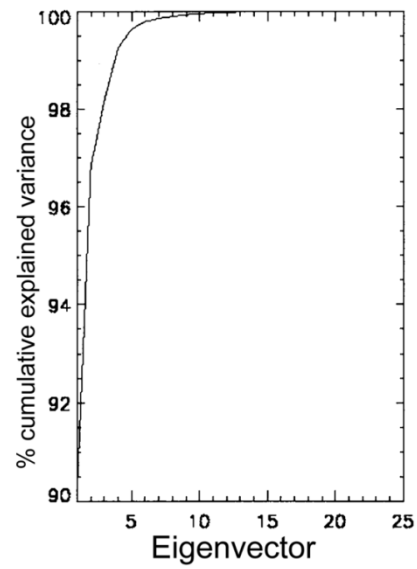

Fig. 1. Cumulative explained variance as a function of the number of eigenvectors.

where $\mathbf{r}$ is the vector of centered (departure from the mean) normalized radiances. Equation (3) is used to reconstruct the radiances from a truncated set of k eigenvectors $\mathbf{E}^*$ and a vector of principal component scores $\mathbf{p}^*$ (the symbol $*$ indicated that the matrix or the result of a matrix operation is due to truncated set of vectors)

$$\mathbf{r}^* = \mathbf{E}^*\mathbf{p}^*. \tag{3}$$

The normalized reconstructed radiance vector is $\mathbf{r}^*$; $\mathbf{E}^*$ has dimension $n \times k$; and the vector $\mathbf{p}^*$ has length k. To obtain the unscaled radiance, one must add the ensemble mean normalized radiance used in generating the covariance matrix and multiply the sum by the noise used in constructing the normalized radiances.

Fig. 1 shows the explained variance of the data with respect to the number of eigenvectors. The eigenvectors were generated from all-sky (cloud-contaminated) AIRS radiances simulated from the six-hour NCEP forecast for December 10, 2000. The explained variance is simply the accumulation of the eigenvalues normalized by the sum of all eigenvalues. Fig. 1 shows that nearly 100% of the variance is explained with only ten eigenvectors. This number is often referred to as the number of independent pieces of information. However, ten eigenvectors are insufficient to reconstruct the radiances within the instrument noise level. A better way to determine the number of eigenvectors is to look at the square root of the eigenvalue, shown in Table I. The square root of the eigenvalues is equivalent to the standard deviation of the principal component scores of the dependent ensemble. Since we are using normalized radiances, the square root of the eigenvalues can be interpreted as signal-to-noise. Principal component scores can be thought of as superchannels, since each one is a linear combination of all channels. The first score contains the largest SNR, which as shown in Table I is very large. When the eigenvalues fall below unity, the noise has larger contribution than the signal. One can argue that no more than 60 or so eigenvectors should be used for

TABLE I
SQUARE ROOT OF THE FIRST 72 EIGENVALUES

Square Root of Eigenvalues (first 72)							
1	7497.60	19	14.68	37	3.38	55	1.25
2	1670.40	20	13.49	38	3.11	56	1.19
3	945.52	21	12.28	39	2.82	57	1.16
4	496.01	22	11.32	40	2.53	58	1.15
5	284.01	23	10.70	41	2.41	59	1.09
6	266.30	24	9.08	42	2.39	60	1.05
7	156.95	25	8.24	43	2.34	61	1.02
8	139.67	26	7.85	44	2.24	62	0.98
9	88.27	27	6.77	45	2.03	63	0.90
10	72.83	28	5.98	46	1.86	64	0.86
11	60.03	29	5.83	47	1.78	65	0.81
12	53.42	30	5.39	48	1.71	66	0.80
13	45.01	31	5.34	49	1.65	67	0.78
14	39.72	32	4.98	50	1.61	68	0.77
15	34.54	33	4.34	51	1.54	69	0.73
16	26.57	34	4.09	52	1.52	70	0.72
17	22.62	35	3.62	53	1.35	71	0.70
18	17.60	36	3.48	54	1.34	72	0.66

reconstructing AIRS spectra. By using a truncated set of eigenvectors much of the noise in the original measurement can be removed. (We decided to save and distribute 200 principal component scores to assure that there was sufficient information to reconstruct real AIRS data.)

The noise filtering aspect of reconstructing radiances using PCA is still being studied. The results are very promising. Fig. 2 shows the AIRS instrument noise at scene brightness temperature, and the rms difference between reconstructed brightness temperatures, from 60 principal component scores, and noise-free simulated brightness temperatures. To compute these results, we simulated brightness temperatures from a global ensemble with and without expected instrument noise. The reconstructed brightness temperatures are computed from the instrument noise-contaminated data. The original noise curve in Fig. 2 is simply the rms difference of the two datasets (noise and noise-free). The rms difference between the reconstructed brightness temperatures and the noise-free simulated brightness temperatures is extremely small in comparison to the instrument noise. The reconstructed data are more similar to noise-free observations. More work is needed to study the impact of using reconstructed radiances in a retrieval algorithm or in radiance assimilation. Since the reconstructed rms difference is very small, we can use the reconstructed data to estimate the noise. This is done by simply computing the rms difference between the reconstructed brightness temperatures and the original noisy data. The difference between the original noise curve in Fig. 2 and the noise estimate using PCA is shown in Fig. 3. The difference is extremely small and therefore this technique can possibly be used as a procedure to estimate instrument noise.

An overall measure of how well the principal component scores can reconstruct the original data is provided by the reconstruction score (RS) which is defined as

$$\mathrm{RS} = \left[\frac{1}{N}\sum_{I=1}^{N}(O_i - R_i)^2\right]^{1/2} \tag{4}$$

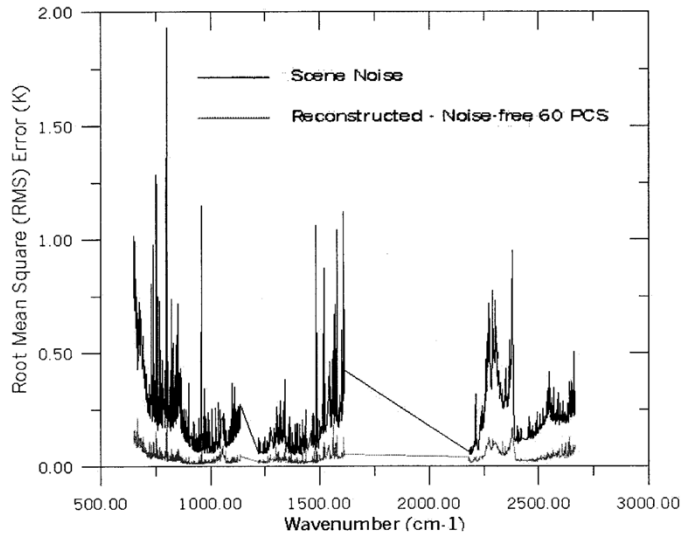

Fig. 2. RMS difference of noise minus noise-free brightness temperatures (scene noise) and rms of reconstructed brightness temperatures from 60 principal component scores minus noise free brightness temperatures.

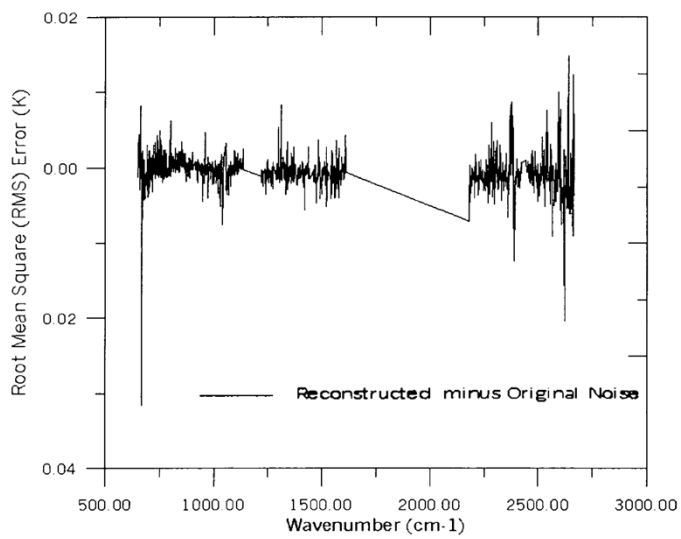

Fig. 3. Difference between the rms of reconstructed brightness temperatures from 60 principal component scores minus noise-contaminated brightness temperature and the scene noise (Fig. 2).

where O and R are the noise-scaled observed and reconstructed radiances, respectively, for the ith channel, and N is the total number of channels used in the principal component analysis. A reconstruction score of less than one indicates that the root-measure-square difference over the number of reconstructed channels is within the noise level. Large reconstruction scores also can be used to identify suspicious data. The mean reconstruction score using 200 principal component scores, for a global ensemble, is about 0.96 with a standard deviation of 0.2. Fig. 4(a) and (b) shows the RS as a function of eigenvector; Fig. 4(b) is an expanded view of Fig. 4(a). Here we see that unity is reached near the 60th eigenvector. One can either examine the eigenvalues or RS to estimate the number of principal component scores needed to reconstruct the radiances to the noise level.

PCA compression provides a way to reconstruct entire AIRS spectra from a much smaller set of data. The eigenvectors are

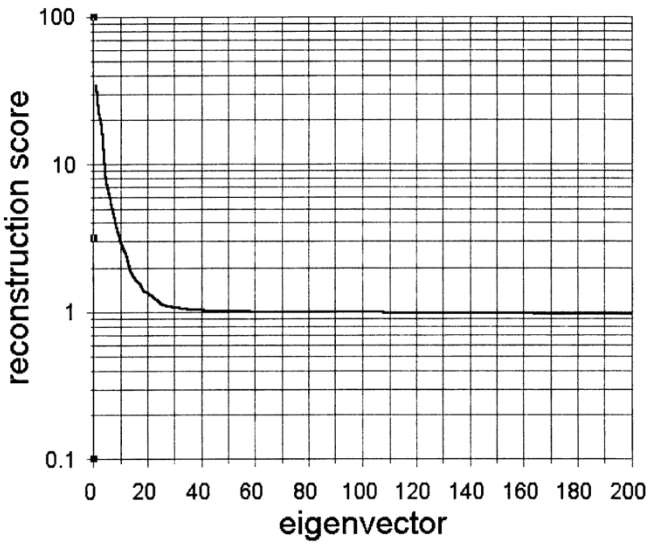

(a)

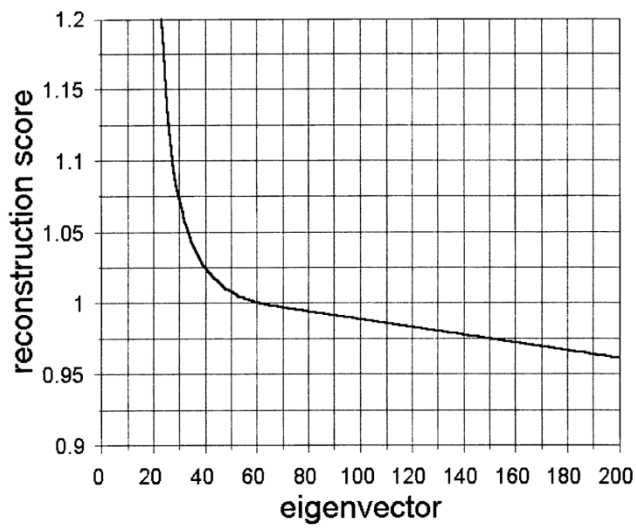

(b)

Fig. 4. Reconstruction score as a function of the number of eigenvectors.

provided in a separate dataset and are static until a new set is computed (see Section III-D). The complete spectra can then be reconstructed. Section III-B discusses principal component regression which provides the initial state for the final physical retrieval [13]. It can also be used as a standalone retrieval.

B. Principal Component Regression

Principal component regression simply uses principal component scores for predictors in least squares regression. For AIRS, we use 60 principal component scores for predictors and solve for atmospheric temperature, moisture, ozone profiles, and surface temperature and surface emissivity. With 2000+ channels, many of the channels are similar to each other, making the covariance matrix nearly collinear. A significant advantage for using 60 principal component scores instead of all 2000+ channels is that the inverse of the predictor matrix is more stable and less collinear. Another advantange is that the regression solution is computationally fast. In matrix notation, the form of the regression coefficients C, dimensioned m number of parameters by the k number of principal component scores, is

$$\mathbf{C} = \mathbf{X}\mathbf{P}^{*^{\mathbf{T}}}\left(\mathbf{P}^{*}\mathbf{P}^{*^{\mathbf{T}}}\right)^{-\mathbf{1}} \tag{5}$$

where $\mathbf{X}$ is a training-dependent predictand ensemble matrix, of dimension m by sample size s. $\mathbf{P}^*$, the training predictor ensemble matrix, is dimensioned k by s. On independent data the m-dimensioned solution vector is obtained from the matrix multiplication of $\mathbf{C}\mathbf{p}^*$, where $\mathbf{p}^*$ is the independent vector of principal component scores of length k.

For this paper, regression coefficients were derived from simulated AIRS data. In practice, the use of simulated data to generate "synthetic" regression coefficients for application on observed data may lead to large biases in the retrieval due to differences between measured and simulated spectra. The AIRS physical retrieval may require a radiance bias adjustment to account for these differences. Initially, the regression coefficients will be based on observed (clear and/or cloud-cleared) principal component score vectors collocated with estimates of the true atmospheric profiles and surface properties, and therefore the solution will need no adjustments to account for differences between measured and computed spectra. Clear observations will be determined using tests described in Section III-E. Derivation of cloud-cleared radiances from FOVs containing broken clouds is described in [16]. If it is later shown that biases between measured and computed spectra can be easily accounted for, then the regression coefficients will be derived from simulated data (i.e., synthetic regression). If "observational" regression (i.e., collocated "truth" and observed AIRS) is used to generate coefficients, then "truth" data will come from collocated radiosonde data or NWP analysis fields. The sparsity of radiosondes will require several months of data to generate a training dataset. The use of analysis fields has the advantage that only one day of data is sufficient to generate coefficients. However, the tradeoff is that the analysis field may have large errors in certain regions. We plan to exclude data from those regions of the analysis field where the absolute differences between the simulated (from NWP model data) AMSU/HSB brightness temperatures and the observed AMSU/HSB brightness temperatures are greater than a predetermined threshold. The threshold will be channel dependent. Synthetic regression will be used for geophysical parameters where the "truth" for the predictands in (5) is not available or extremely sparse (e.g., surface emissivity, skin temperature, upper stratospheric temperature, upper atmospheric water vapor). In the case of collocated radiosondes, synthetic regression is used above the nominal vertical extent of radiosondes (about 10 mb).

AIRS viewing geometry changes along the scanline. Coefficients are computed for different ranges of viewing geometry to account for the limb effect. The limb effect is due to the increased absorption due to the increase in optical path. The measurements become more opaque with increasing scan angle. We divided the AIRS data in intervals of 0.1 of the cosine (scan

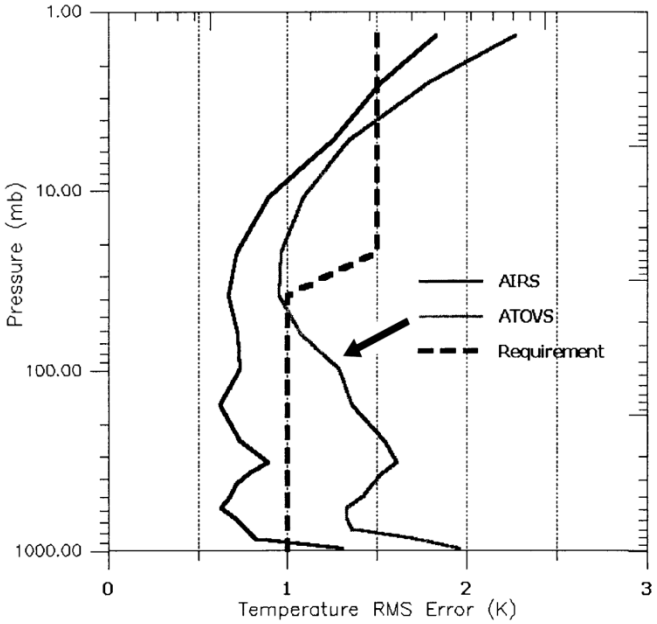

Fig. 5. Comparison of regression retrieval temperature rms errors from AIRS and ATOVS.

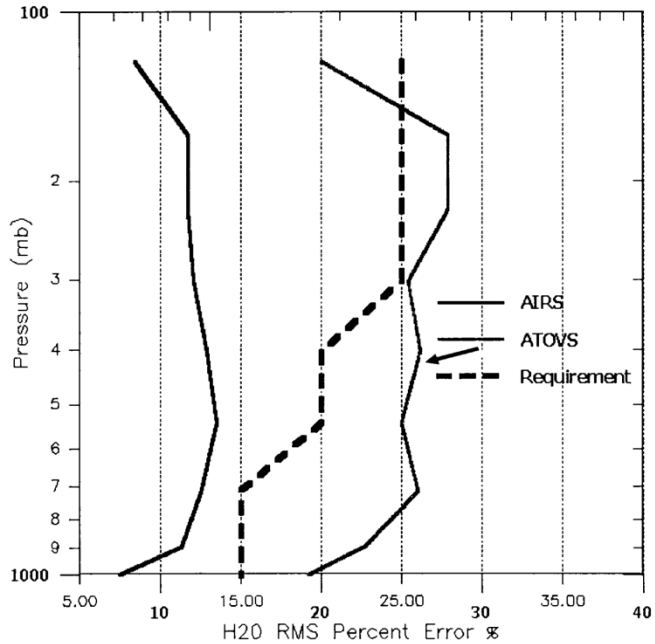

Fig. 6. Comparison of retrieval water vapor rms percent error from AIRS and ATOVS.

angle). There are four intervals. Each interval and all geophysical parameters use the same predictors: 60 principal component scores, unity minus cosine (scan angle), and side of scan (one for left, zero for right). The side of scan is used to account for possible scan asymmetries in the observations. It should be pointed out that an earlier form of the regression used limb adjusted principal component scores. This approach worked quite well in simulation; however, in practice, the limb adjustment coefficients may need to be based on real data and would require considerable resources to collect the data to generate the coefficients. It was shown in [22] that the limb adjustment for AMSU-A resulted in adjusted observations that were nearly indistinguishable from nadir values. Theoretically, limb adjusting AIRS should work extremely well because AIRS has so many overlapping weighting functions. We have not ruled out this option, but we prefer the current approach because we should be able to produce acceptable regression retrievals very quickly after the AIRS level 1 b data have been verified.

Figs. 5 and 6 show a comparison of expected regression temperature and moisture profile accuracy, respectively, from AIRS and ATOVS. The results are based on simulated radiances. The ensemble used was obtained from a collection of radiosonde atmospheric temperature and moisture profiles and Dobson stations for atmospheric ozone. The upper stratospheric temperatures were obtained from rocketsondes. Surface temperature was derived from the HIRS window channels. Random surface emissivity with a mean of 0.98 and a standard deviation of 0.1 was used over land. The Masuda surface emissivity model [23] was used over ocean. Appropriate instrument noise values were added to the simulated radiances. The dashed line in both curves shows the required performance. The temperature accuracy from AIRS, as expected, is much better than from ATOVS. The use of a physical retrieval [16] considerably improves the lower tropospheric temperatures. The moisture accuracy from AIRS is significantly better than those from ATOVS. AIRS has near-continuous moisture information between 6 and 8 μm at high spectral resolution, whereas ATOVS has only a few relatively broad channels. Fig. 7 show ozone performance. In this figure, the mean, in Dobson, and standard deviation of the mean, in percent, are shown, along with the retrieval accuracy. Overall, the ozone retrieval has an error of about 10% at the standard Umkehr layers ($\sim$5-km thickness). The total integrated ozone layer is about 3.5%. The above results are for clear conditions. Retrieval performance from cloud-cleared radiances is reported in [16].

The AIRS Science Team simulation of December 15, 2000 was used to test our surface emissivity regression retrieval. Details on the modeling of land surface emissivity in the simulation are described in [18]. Fig. 8 shows the standard deviation of the true emissivity and the retrieval error for December 15, 2000 for land surfaces. The overall emissivity retrieval error is within 0.5% of the "true" emissivity used in the simulations. Over ocean, the Masuda surface emissivity model is used. The surface skin temperature error for all surfaces, based on clear simulations, is approximately 0.3 K.

C. Local Angle Adjustment

An array of 3×3 AIRS FOVs within an AMSU-A FOV is used to cloud-clear AIRS radiances under conditions of broken clouds. The 3×3 array has three columns of three AIRS observations. Each column has a different view angle. The cloud-clearing algorithm [16] assumes that differences between the nine FOVs are only due to clouds. Therefore, differences due to viewing geometry must be removed. The observations from each of the outer columns are adjusted to the angle of the middle column. Principal component regression is used to derive the local angle adjustments.

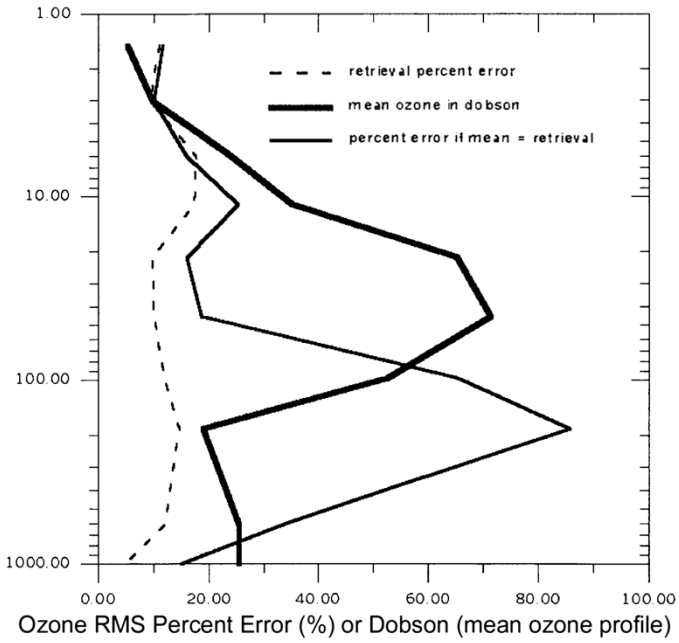

Fig. 7. Ozone retrieval rms percent errors (dashed), background error in percent (thin line), and mean ozone for ensemble (thick line).

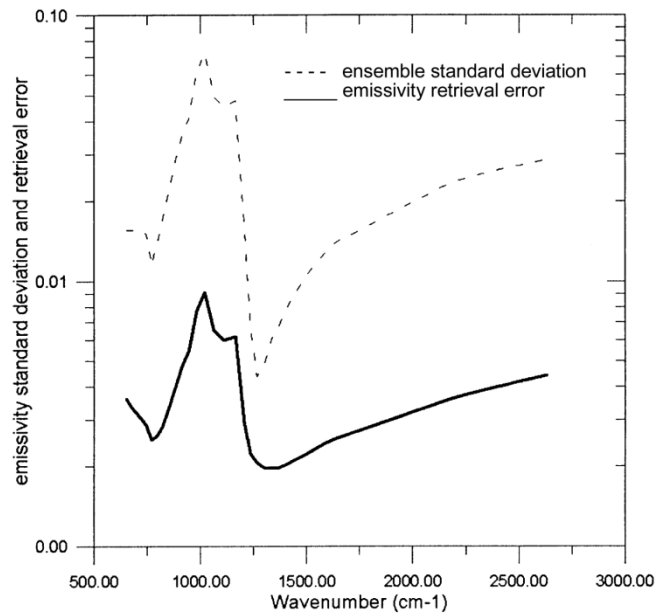

Fig. 8. Standard deviation of emissivity spectra in training ensemble and the standard deviation of the emissivity retrieval error.

The AIRS local angle adjustment is based on simulated values. That is, a sample of profiles was used to calculate radiances for multiple cloud conditions and angles to produce regression coefficients that use the observed principal component scores to predict the angle adjustments. We made an important improvement in our simulation. When we first calculated adjustments, we noted that the adjusted error for the center angles was significantly larger than the adjustment itself, which is nearly zero for adjacent spots near the center of the scan. We then realized that the original simulation was flawed in the way the instrument noise was handled. What should be simulated is the measurement that would have been observed had the instrument been observing at a different angle with all other parameters the same. This means that the noise that would have been observed at the new angle is the same as the one that was observed at the given angle. To create this feature, a single noise value was used for all angles for a given profile. The noise changed with profile, cloud, etc. in the usual way. This seems like a small detail, but it had a significant effect on the accuracy of the angle adjustments. In particular, the error in the adjustments for the center spots became consistent with the size of the observed angle effects in that it was no longer larger than the largest expected correction.

D. Updating of Eigenvectors and Regression Coefficients

Our strategy for updating eigenvectors and regression coefficients starts from an initial training set. Those eigenvectors and coefficients are then referred to as the static set. We will first discuss updating the regression coefficients. New principal component score regression coefficients will be generated periodically, perhaps daily if the NWP model is used for training the regression retrieval. However these coefficients are never used to derive the "official" product, they're only used to monitor the static coefficients and to find outliers that may need to be added to the original training. Results from the new coefficients will be compared in an offline mode with results based on the static coefficients. If a certain number of outliers are found, those that are more than 2.5 standard deviations away from the mean and with populations much greater than expected from a normal population, then the outlier population is added to the static training set and coefficients are regenerated.

The data used for generating the eigenvectors are derived from an offline dataset consisting of three of the 135 scanlines per granule (scanlines 2, 47, and 92). There are 240 6-min granules per day and each scanline contains 90 AIRS FOVs. We use every third AIRS spots from spot 2 through 89, which matches the spatial sampling provide in the single FOV dataset, described in Section II-A. So each day there are 21 600 spectra ($30 \times 3 \times 240$), and from that set we select a smaller subset that is approximately one third of the 21 600. Eigenvectors are computed daily, but they are only used to monitor the representativeness of the static set of eigenvectors by comparing reconstruction scores derived from the static and updated eigenvectors. We have tested this approach in our near-real-time system, based on simulated data, and found that the first update of the static set occur in about three weeks with the frequency gradually reducing to the point that in six months there is no need to further update the static set (assuming that the AIRS instrument remains stable).

E. Detecting Clear Fields of View

The determination of cloud-free AIRS FOVs is very important for two important reasons. First the initial testing of the AIRS retrieval package after launch will be done on clear-only FOVs. The determination of these clear FOVs is important for the initial generation of regression coefficients. Second, some NWP centers will assimilate only FOVs that are free of clouds. A clear FOV indicator is included in the product files. The methodology to determine clear FOVs differs between ocean

and land surfaces. The following two subsections will discuss them. It should be noted that AIRS also has a visible/near infrared (Vis/NIR) instrument with a spatial resolution on the ground of about 2.28 km. As discussed in [24], the Vis/NIR instrument can provide information on cloud contamination within the approximately 14-km AIRS FOV. An AIRS Vis/NIR cloud indicator will also be available in the product files. This paper will address cloud detection based only on AIRS and AMSU-A observations. The cloud detection tests can be considered preliminary, since they were developed with simulated data. The utilization of real AIRS data will likely lead toward the development of additional tests, which were not developed because of limitations in the simulated data. For example, the AIRS simulations did not include realistic spectrally varying cloud emissivity, so tests examining spectral characteristics of clouds were not developed.

1) Clear Detection Over Ocean: Clear detection over ocean involves five different tests. The FOV must pass all five tests to be declared clear. Test 1 simply checks if brightness temperature at a single longwave window channel at 965.43 cm^{-1} is warmer than 270 K. (Note that the channel frequencies will be slightly different for the real AIRS observations.) If it is less than 270 K, it is almost certain that clouds are present, since the freezing temperature of sea water is near 271 K. Test 2 checks the difference between the sea surface temperature (SST) from the NCEP six-hour forecast with a nearly transparent shortwave window channel at 2616.095 cm^{-1}. The 2616-cm^{-1} channel is the most transparent AIRS window channel. The atmospheric component is less than 0.5 K, and the instrument noise is very low (less than 0.05 K for a surface temperature of 280 K). Tests involving this channel can only be performed with night data due to solar contamination. If the brightness temperature from the 2616-cm^{-1} channel is more than some threshold (e.g., 1 K) colder than the SST, it is assumed that there are some clouds in the FOV. Tests 3 and 4 use least squares regression to predict the 2616-cm^{-1} channel from several 8- and 11-μm split window channels, respectively. The 8-μm channels used are at 1218.36, 1228.09, 1236.40, and 1251.21 cm^{-1}, and the 11-μm channels used are at 918.65 and 965.32 cm^{-1}. The channels were selected by stepwise regression. The 2616-cm^{-1} channel can be predicted from either the set of 8- or 11-μm channels with an accuracy of about 0.5 K. Both regressions also use cosine(scan angle) as an additional predictor. Because of the nonlinear relationship between Planck radiance and temperature in the infrared, the 2616-cm^{-1} channel is less sensitive to partial cloudiness than the 11- and 8-μm channels. For example given 50% single cloud cover with a cloud-top temperature of 220 K and a surface temperature of 280 K, the brightness temperature at 2616.10, 1251.21, and 918.65 cm^{-1} are 266.7, 258.6, and 255.8, respectively. The brightness temperatures from the 2616-cm^{-1} channel, and the longwave window channels are similar only for clear sky and uniform overcast conditions. So if the difference between the predicted 2616-cm^{-1} channel and the observed is greater than some threshold, then the FOV is not clear. The 11- and 8-μm channels are used separately because it was observed when used together the different degree of Planck nonlinearity of the 11- and 8-μm channels would actually predict the 2616-cm^{-1} channel brightness temperature very accurately in conditions of low cloud amount. Test 5 predicts the NCEP SST from 8- and 11-μm split window channels (used together in the prediction). The predictor channels are 918.65, 965.32, 1228.09, and 1236.40 cm^{-1}. Again cosine (scan angle) is used as an extra predictor. If the predicted SST is colder than the NCEP SST, then the FOV has cloud contamination. The selection of thresholds for the above tests can be estimated using cumulative distribution functions. For example, Fig. 9(a) and (b) shows the cumulative distribution function of the difference between SSTs and the brightness temperatures observed by the 2616-cm^{-1} channel (test 2). If 5% of the ocean is assumed clear, then this approach would select 0.9 K as the threshold. We plan to use Moderate-Resolution Imaging Spectroradiometer (MODIS) cloud mask to determine the expected percentage of clear data at the AIRS spatial resolution.

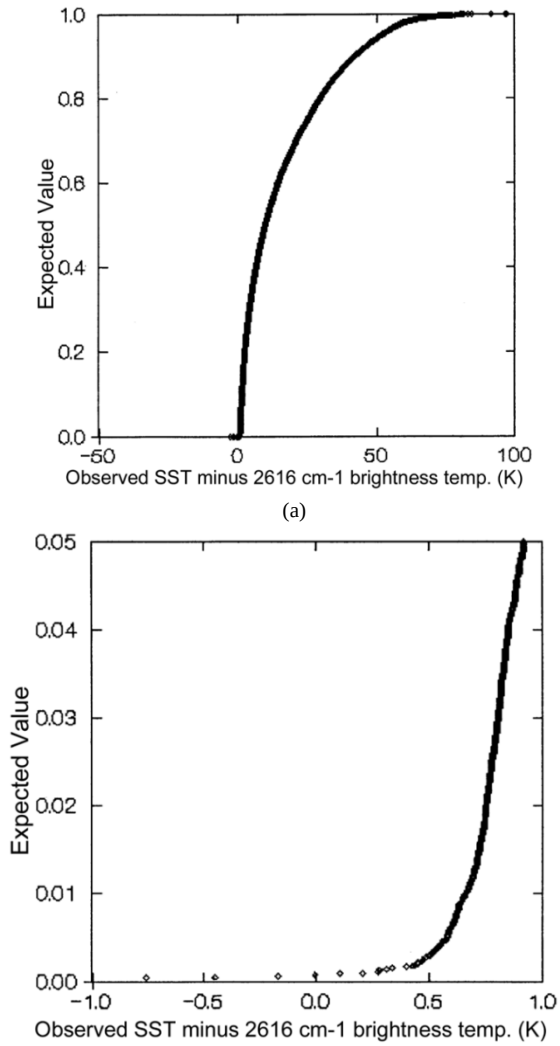

Fig. 9. Cumulative distribution function of the difference between SSTs and the brightness temperatures observed by the 2616-cm^{-1} channel.

The above tests were applied to AIRS/AMSU/HSB data simulated for December 15, 2000. Only 4.5% of the total number of FOVs passed the clear tests The simulations included two layers of clouds and the overall mean cloud amount was 45% with a standard deviation of 33%. The mean residual cloud fraction in the FOVs detected as clear is near 0.006 (1 = total overcast)

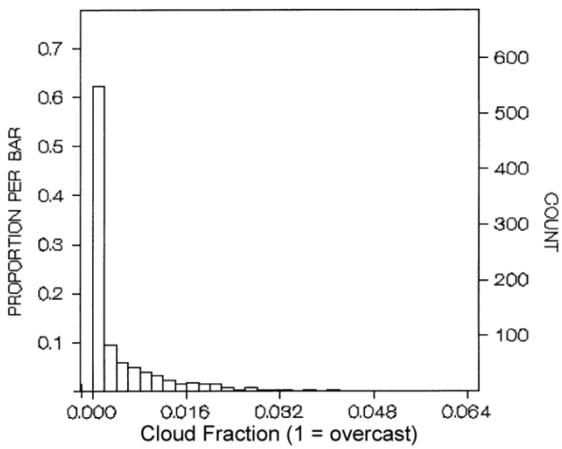

Fig. 10. Histogram of residual cloud amount for cases passing the clear test.

and the standard deviation is about 0.009. A histogram of the residual cloud amount is in Fig. 10.

2) Clear Detection Over Land: Greater uncertainty in land surface emissivity and relatively poor forecast surface temperature from land surfaces prevents the use of the tests that were developed for AIRS data over the ocean. The land tests make use of AMSU-A and the spatial variability of the 3×3 AIRS FOVs in the AMSU-A FOV. Test 1 predicts a single AIRS channel at 2390 cm^{-1} from AMSU-A channels 4 though 6. The coefficients are derived from simulated data. The 2390-cm^{-1} channel can be predicted from AMSU-A with an accuracy of about 1 K. The weighting function for this particular AIRS channel, which has a peak value near 850 mb, is given in Fig. 11. The 2390-cm^{-1} channel is ideal, because it is predominately affected by temperature; contamination from water vapor and other trace gases is negligible. Simulations have shown that this channel is only marginally affected by solar contamination ($<$0.1 K) for clear conditions. Ideally, a channel peaking lower in the troposphere would be better for detecting very low altitude clouds. However, predicting near-surface AIRS channels would require the use of AMSU-A window channels. The large variability of the AMSU-A window channels due to variations in cloud liquid water and surface emissivity result in a very poor prediction ($>$5 K) of near-surface AIRS channels. Test 1 compares the predicted 2390-cm^{-1} channel with the observed, if the observed is colder by some threshold (e.g., 2 K) then the AIRS FOV is not cloud-free. For overcast conditions during the day, solar contamination can result in a warm brightness temperature. To avoid false detection of clear FOVs due to solar contamination of the 2390-cm^{-1} channel in presence of clouds, Test 2 was added to compare the difference of brightness temperatures from 2558.23 and 937.81 cm^{-1}. If the difference is greater than 10 K, the FOV is not cloud-free. Experiments have found that FOVs with very low level clouds are often not detected. This of course was expected, since the 2390-cm^{-1} channel peaks near 850 mb. To improve the detection of very low clouds, Test 3, the coherence test, computes the standard deviation of the 3×3 array of the 2390-cm^{-1} channel radiance within the AMSU-A FOV. Radiance is used instead of brightness temperature because the noise is temperature dependent. If the

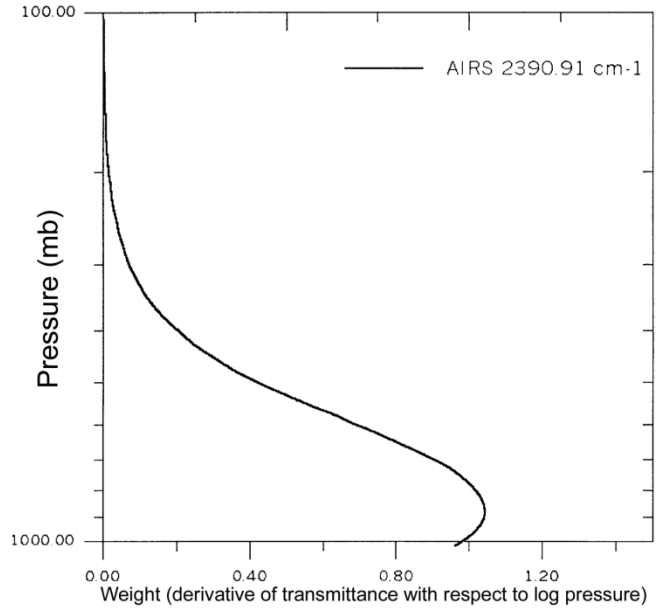

Fig. 11. Weighting function of the AIRS channel near 2390 cm^{-1}.

standard deviation is greater than three times the noise, then the FOV is not cloud-free. This test can produce false positives in regions of high and variable terrain. Test 4 is similar in concept to tests 3 and 4 in Section III-E-1. However, because of variable surface emissivity, a channel peaking near 950 mb (2445.92 cm^{-1}) is used instead of a shortwave infrared window channel. Test 4 uses the same predictor channels as Test 3 in Section III-E-I. Test 5 is similar to Test 5 in Section III-E-I; however, since the forecast skin temperature is rather poor over land surfaces, a very large threshold is used (e.g., 10 K).

The detection of clear over land is not nearly as good as those obtain for ocean cases. The overall cloud residual error is about 2.5%. If the coherence test was not included, the residual cloud would be about 8%. The entire AMSU-A FOV needs to be clear for the coherence test to pass. Fig. 12(a) and (b) shows the scatter diagram of cloud amount and cloud top pressure for FOVs that are thought to be clear using only land test 1 (AMSU-A prediction of AIRS) and the improvement using the coherence test, respectively. Use of a high spatial resolution imager, such as MODIS would considerably improve clear detection over land. The MODIS has infrared channels, similar to those of HIRS, however with a spatial resolution of 1 km. We are planning, as a future enhancement to the AIRS real-time processing system, to use MODIS to improve cloud detection and cloud clearing. Cloud clearing requires a clear estimate of selected AIRS channels [16]. The current algorithm uses AMSU-A to derive the clear estimate. The high spatial resolution MODIS can be used to find a clear MODIS FOV within the AIRS FOV containing broken clouds. The AIRS clear estimate is then derived from the clear MODIS infrared channels.

IV. Summary

AIRS radiance and retrieval products will be available to the NWP community in near-real-time. Principal component regression provides a very computationally efficient retrieval

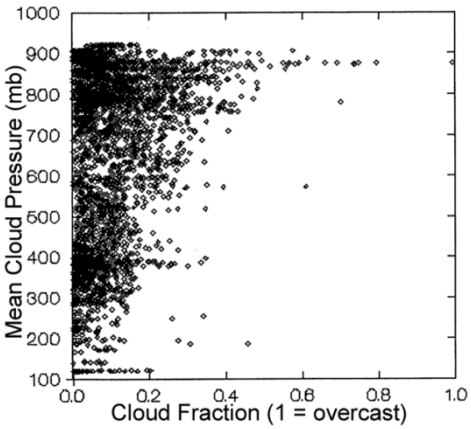

(a)

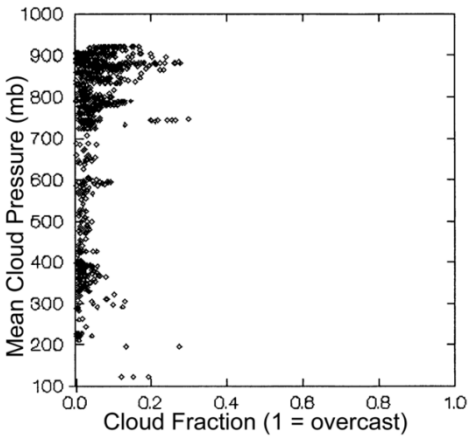

(b)

Fig. 12. (a) Residual clouds using only AMSU-A test and (b) residual clouds using both AMSU-A and spatial variability tests (b).

of atmospheric temperature, moisture, and ozone, as well as surface parameters, such as skin temperature and emissivity. The regression retrieval, also referred to as the initial retrieval, is used as the first guess in the AIRS physical retrieval. Principal component scores can also be used for data compression, since we have demonstrated that 2000+ AIRS channels can accurately be reconstructed from 60 scores. The noise-filtering feature of reconstructed radiances is very promising and we strongly encourage NWP centers to experiment with assimilating reconstructed AIRS radiances. We plan to apply reconstructed radiances to the AIRS physical retrieval. The thinned radiance and principal component score files provide the options for NWP centers to use either observed or reconstructed noise-filtered radiances. Cloud detection tests are available to estimate clear AIRS FOVs, although these constitute less than 5% of the FOVs. Because of this very low yield, we also strongly encourage experiments directed toward assimilating cloud-cleared radiances.

REFERENCES

[1] H. H. Aumann, M. T. Chanhine, C. Gautier, M. D. Goldberg, E. Kalnay, L. M. McMillin, H. Revercomb, P. W. Rosenkranz, W. L. Smith, D. H. Staelin, L. L. Strow, and J. Susskind, "AIRS/AMSU/HSB on the AQUA mission: Design, science objectives, data products, and processing systems," *IEEE Trans. Geosci. Remote Sensing*, vol. 41, pp. 253–264, Feb. 2003.

[2] T. S. Pagano, H. H. Aumann, D. E. Hagan, and K. Overoye, "Prelaunch and in-flight radiometric calibration of the Atmospheric Infrared Sounder (AIRS)," *IEEE Trans. Geosci. Remote Sensing*, vol. 41, pp. 265–273, Feb. 2003.

[3] W. L. Smith, H. Woolf, C. Hayden, D. Wark, and L. McMillin, "The TIROS-N operational vertical sounder," *Bull. Amer. Meteorol. Soc*, vol. 60, pp. 1177–1187, 1979.

[4] K. B. Kidwell, *NOAA KLM Users Guide: NOAA Polar Orbital Environmental Satellites (POES)*. Washington, DC: U.S. Dept. of Commerce. National Oceanic and Atmospheric Admin., Satellite Data Services Div., 2000.

[5] P. Prunet, J.-N. Thepaut, and V. Casse, "The information content of clear sky IASI radiances and their potential for numerical weather prediction," *Q. J. R. Meteorol. Soc.*, vol. 124, pp. 211–242, 1998.

[6] E. Andersson, J. Pailleux, J. N. Thepaut, J. R. Eyre, A. P. McNally, G. A. Kelly, and P. Courtier, "Use of cloud-cleared radiances in three/four dimensional variational data assimilation," *Q. J. R. Meteorol. Soc.*, vol. 120, pp. 627–653, 1994.

[7] J. C. Derber and W.-S. Wu, "The use of TOVS cloud-cleared radiances in the NCEP SSI analysis system," *Mon. Weather Rev.*, vol. 126, pp. 2287–2299, 1998.

[8] A. P. McNally, J. C. Derber, W.-S. Wu, and B. B. Katz, "The use of TOVS level-1B radiances in the NCEP SSI analysis system," *Q. J. R. Meteorol. Soc.* , vol. 126, pp. 689–724, 2000.

[9] S. J. English, R. J. Renshaw, P. C. Dibben, A. J. Smith, P. J. Rayer, C. Poulsen, F. W. Saunders, and J. R. Eyer, "A comparison of the impact of TOVS and ATOVS satellite sounding data on the accuracy of numerical weather forecasts," *Q. J. R. Meteorol. Soc.*, vol. 126, pp. 2911–2931, 2000.

[10] J. C. Derber, "The use of ATOVS data at NCEP," in *Proc. ECMWF/EUMETSAT Workshop on the Use of ATOVS Data for NWP Assimilation*, Reading, U.K., 1999, pp. 33–38.

[11] A. P. McNally and G. Kelly, "The use of raw TOVS/ATOVS radiances in the ECMWF 4-D assimilation system," in *Proc. ECMWF/EUMETSAT Workshop on the Use of ATOVS Data for NWP Assimilation*, Reading, U.K., 1999, pp. 23–32.

[12] W. L. Smith, "An improved method for calculating tropospheric temperature and moisture from satellite radiometer measurements," *Mon. Weather Rev.*, vol. 96, pp. 387–396, 1968.

[13] M. T. Chahine, "Remote sounding of cloudy atmospheres I. The single cloud layer," *J. Atmos. Sci.*, vol. 31, pp. 233–243, 1974.

[14] ——, "Remote sounding of cloudy atmospheres II. Multiple cloud layer," *J. Atmos. Sci.*, vol. 31, pp. 744–757, 1977.

[15] L. M. McMillin and C. Dean, "Evaluation of a new operational technique for producing clear radiances," *J. Appl. Meteorol.*, vol. 21, pp. 1005–1014, 1982.

[16] J. Susskind, C. D. Barnet, and J. M. Blaisdell, "Retrieval of atmospheric and surface parameters from AIRS/AMSU/HSB data in the presence of clouds," *IEEE Trans. Geosci. Remote Sensing*, vol. 41, pp. 390–409, Feb. 2003.

[17] F. Chevallier, P. Bauer, J.-F. Mahfouf, and J.-J. Morcrette, "Variational retrieval of cloud profile from ATOVS observations," *Q. J. R. Meteorol. Soc.*, vol. 128, pp. 2511–2526, 2002.

[18] E. Fishbein, C. B. Farmer, S. L. Granger, D. T. Gregorich, M. R. Gunson, S. E. Hannon, M. D. Hofstadter, S.-Y. Lee, S. S. Leroy, and L. L. Strow, "Formulation and validation of simulated data for the Atmospheric Infrared Sounder (AIRS)," *IEEE Trans. Geosci. Remote Sensing*, vol. 41, pp. 314–329, Feb. 2003.

[19] D. Q. Wark and H. E. Fleming, "Indirect measurements of atmospheric temperature profiles from satellites I. Introduction," *Mon. Weather Rev.*, vol. 94, pp. 351–362, 1966.

[20] W. L. Smith and H. M. Woolf, "The use of eigenvectors of statistical covariance matrices for interpreting satellite sounding radiometer observations," *J. Atmos. Sci.*, vol. 33, pp. 1127–1203, 1976.

[21] H.-L. Huang and P. Antonelli, "Application of principal component analysis to high-resolution infrared measurement compression and retrieval," *J. Appl. Meteorol.*, vol. 40, pp. 365–388, 2001.

[22] M. D. Goldberg, D. S. Crosby, and L. Zhou, "The limb adjustment of AMSU-A observations: Methodology and validation," *J. Appl. Meteorol.*, vol. 40, pp. 70–83, 2001.

[23] K. Masuda, T. Takashima, and Y. Takayama, "Emissivity of pure and sea waters for the model sea surface in the infrared window regions," *Remote Sens. Environ.*, vol. 24, pp. 313–329, 1988.

[24] C. Gautier, Y. Shiren, and M. D. Hofstadter, "AIRS/Vis Near IR instrument," *IEEE Trans. Geosci. Remote Sensing*, vol. 41, pp. 330–342, Feb. 2003.

Mitchell D. Goldberg received the B.S. degree from Rutgers University, New Brunswick, NJ, in 1981, and the M.S. degree from the University of Maryland, College Park, in 1984, both in in meteorology.

He is currently with the National Oceanic and Atmospheric Administration, National Environmental Satellite, Data, and Information Service, Office of Research and Applications, Camp Springs, MD, and is currently the chief of the Climate Research and Applications Division. His area of expertise is satellite-based passive infrared and microwave remote sensing. He has developed retrieval algorithms for deriving atmospheric temperature and moisture profiles from observations made by the HIRS, AIRS, MSU, and AMSU instruments. The products derived from these algorithms are used in weather and climate applications.

Yanni Qu received the Ph.D. degree in atmospheric science from the University of Wisconsin, Madison.

Her area of expertise is deriving geophysical parameters from satellite hyperspectral infrared observations. She currently works on algorithm development for the CrIS sensor at ITT, Fort Wayne, IN (Decision Systems Technologies, Inc., Rockville, MD).

Larry M. McMillin received the B.S. and M.S. degrees from the University of Michigan, Ann Arbor, in 1963 and 1966, an the Ph.D. degre from Iowa State University, Ames, in 1971, all in physical meteorology.

He is currently a Research Physical Scientist with the National Oceanic and Atmospheric Administration's National Environmental Satellite, Data, and Information Service, Camp Springs, MD, where he has worked since 1971, and currently works for the Office of Research and Applications. He specializes on instruments used for remote sensing including AIRS, IPO, and TOVS, and methods for processing data from these and similar instruments. He has developed algorithms for measuring sea surface temperatures, cloud-clearing radiances, and rapid calculations of atmospheric transmittances.

Walter Wolf received the B.S. degree from the State University of New York, Albany, and the M.S. degree from the University of Wisconsin, Madison, both in atmospheric science.

He creates operational programs in the field of atmospheric science. In his current position at QSS Group, Inc., Lanham, MD, he has designed, developed, and implemented a software system to deliver near-real-time Aqua satellite data to the global Numerical Weather Prediction Centers. Prior to this, he created the International ATOVS Processing Package (IAPP) that produces global temperature and water vapor retrievals. The IAPP is still being used operationally around the world.

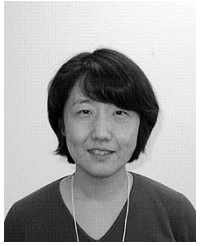

Lihang Zhou received the B.S. degree in physical oceanography from the Ocean University of Qingdao, Qingdao, China, and the M.S. degree in meteorology from the University of Maryland, College Park.

Her main responsibility is to develop, test, and implement NOAA/AIRS science algorithms. She also develops web-based visualization tools to monitor the real-time AIRS/AMSU/HBS processing system. As a test of the AIRS operational system, she wrote programs and scripts for building an AMSU-A operational system. The system, which has functions such as data accessing and processing, visualization of products, and web publishing, has been running successfully since summer 1998. The AMSU-A products are used in hurricane and climate studies.

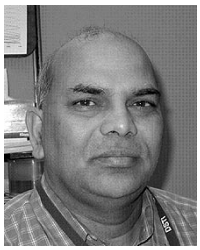

Murty Divakarla received the M.S. and the Ph.D. degrees from the University of Wisconsin, Madison, both in meteorology.

He is presently with Decision Systems Technologies, Inc., Rockville, MD. He was formerly with the Indian Space Research Organization (ISRO), Ahmedabad, India, from 1978 to 1988, and he worked on the retrieval of temperature and moisture profiles using NOAA satellite TOVS data (HIRS, MSU, and SSU). His present interests include the evaluation of high-resolution satellite sounding instruments such as AIRS, IASI *vis-à-vis* fast transmittance models in terms of their agreement with theoretical calculations; and the evaluation of retrieval accuracies for temperature and moisture profiles from IR (AIRS, IASI) and microwave instruments (AMSU) and their sensitivity to different noise levels and channel combinations.